

THE JOSEPHSON BIFURCATION AMPLIFIER FOR QUANTUM MEASUREMENTS

I. Siddiqi, R. Vijay, F. Pierre, C.M. Wilson, L. Frunzio, M. Metcalfe, C. Rigetti, and M.H. Devoret

*Departments of Applied Physics and Physics
Yale University, USA*

irfan.siddiqi@yale.edu

Abstract We have constructed a new type of amplifier whose primary purpose is the read-out of superconducting quantum bits. It is based on the transition of an RF-driven Josephson junction between two distinct oscillation states near a dynamical bifurcation point. The main advantages of this new amplifier are speed, high-sensitivity, low back-action, and the absence of on-chip dissipation. Using pulsed microwave techniques, we demonstrate bifurcation amplification in nanofabricated Al junctions and verify that the performance predicted by theory is attained.

1. Introduction

Josephson first noted that the superconducting tunnel junction can be viewed as a non-linear, non-dissipative, electrodynamic oscillator [1]. We exploit this non-linearity to produce a new type of high-sensitivity amplifier, the Josephson Bifurcation Amplifier (JBA). No shunt resistors are required in our amplification scheme, and it is thus possible to take advantage of the elastic character of the junction and eliminate on-chip dissipation, thereby minimizing the back-action of the amplifier. The combination of high-sensitivity and minimal back-action makes the JBA well-suited for measurements on quantum systems such as superconducting qubits, and make it a strong candidate for reaching the quantum noise limit.

The operation of the JBA is represented schematically in Fig. 1. The central element is a Josephson junction, shunted with a lithographic capacitor, whose critical current I_0 is modulated by an input signal (input port). Coupling between the junction and the input signal can be achieved through different schemes, examples of which involve placing the JBA in a SQUID loop [2] or in parallel with a SSET [3]. The junction is driven with a pure AC signal $i_{RF} \sin(\omega t)$ in the microwave frequency range fed via a transmission

line through a circulator (drive port). In the underdamped regime, for certain values of ω and i_{RF} , two possible oscillation states which differ in amplitude and phase (denoted "0" and "1") can coexist. The reflected component of the drive signal, measured through another transmission line connected to the circulator (output port), is a convenient signature of the junction oscillation state. At the bifurcation point where switching between oscillation states occurs, the system becomes infinitely sensitive, in the absence of thermal and quantum fluctuations, to variations in I_0 . At finite temperature, the energy stored in the oscillation can always be made larger than thermal fluctuations by increasing the scale of I_0 , thus preserving sensitivity. Small variations in I_0 are transformed into readily discernible changes in the escape rate Γ_{01} from state 0 to 1. Back-action is minimized in this arrangement since the only fluctuations felt at the input port arise from the fluctuations of the $50\ \Omega$ drive port whose dissipative elements are physically separated from the junction via a transmission line of arbitrary length and can therefore be thermalized efficiently to base temperature. Additionally, the frequency band over which the back-action contributes is narrow, and well controlled.

In section 2, simplified expressions adapted from the theory of activated escape in a driven non-linear oscillator [4] are presented. Details of the devices and the measurement setup are presented in Section 3. Experimental results are given in Section 3, and concluding remarks are in Section 4.

2. Theory

The tunnelling of Cooper pairs manifests itself as a non-linear inductance that shunts the linear junction self-capacitance C_J , formed by the junction electrodes and the tunnel oxide layer. The constitutive relation of the non-linear inductor can be written as $I(t) = I_0 \sin \delta(t)$, where $I(t)$, $\delta(t) = \int_{-\infty}^t dt' V(t')/\varphi_0$ and $V(t)$ are the current, gauge-invariant phase-difference and voltage corresponding to the inductor, respectively, while the parameter I_0 is the junction critical current. Here $\varphi_0 = \hbar/2e$ is the reduced flux quantum. The dynamics of the junction are given by the time evolution of δ , which exhibits the motion of a phase particle in a cosine potential $U(\delta) = -\varphi_0 I_0 \cos(\delta)$. For small oscillation amplitude about the potential minima, the frequency of oscillation is given for zero DC bias current by the plasma frequency $\omega_{P0} = 1/\sqrt{L_J C_J}$ where $L_J = \varphi_0/I_0$ is the effective junction inductance. As the oscillation amplitude increases, the potential "softens" and ω_P decreases, an effect which has been measured in both the classical and quantum regime [5–8]. A more dramatic non-linear effect manifests itself if the junction is driven with an AC current $i_{RF} \sin \omega t$ at a frequency ω slightly below ω_{P0} . If the quality factor $Q = C_J \omega_{P0} / \text{Re}[Z^{-1}(\omega_{P0})]$ is greater than $\sqrt{3}/2\alpha$, where $Z(\omega_{P0})$ is the impedance of the junction electrodynamic envi-

rument and $\alpha = 1 - \omega/\omega_{P0}$ the detuning parameter, then the junction switches from one dynamical oscillation state to another when i_{RF} is ramped above a critical value I_B [9]. For $i_{RF} < I_B$, the oscillation state is low-amplitude and phase-lagging while for $i_{RF} > I_B$, the oscillation state is high-amplitude and phase-leading. This generic non-linear phenomenon, which we refer to as "dynamical switching", is reminiscent of the usual "static switching" of the junction from the zero-voltage state to the voltage state when the DC current bias exceeds the critical current I_0 [10]. However, an important distinction between dynamical and static switching is that in dynamical switching, the phase particle remains confined to only one well of the junction cosine potential, and the time-average value of δ is always zero. The junction never switches to the voltage state, and thus no DC voltage is generated. Also, for dynamical switching, the current I_B depends both on Q and on the detuning α .

In presence of the microwave drive $i_{RF} \sin(\omega t)$, the oscillations in the junction phase can be parameterized using in-phase and quadrature phase components $\delta(t) = \delta_{\parallel} \sin(\omega t) + \delta_{\perp} \cos(\omega t)$ (higher harmonics of oscillation are negligible). The two oscillation states appear as two points in the $(\delta_{\parallel}, \delta_{\perp})$ plane and are denoted by vectors labelled 0 and 1 (see Fig. 2). The error-current [11]

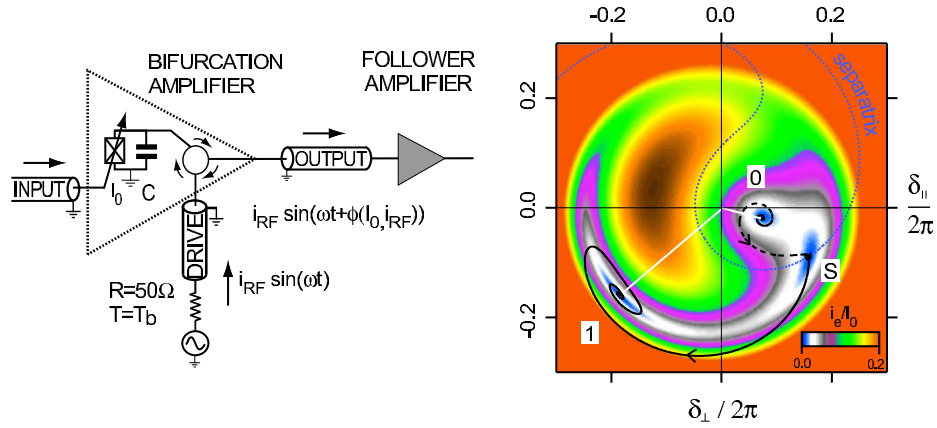


Figure 1. Schematic diagram of the Josephson bifurcation amplifier. A junction with critical current I_0 , parametrically coupled to the input port, is driven by an RF signal which provides the power for amplification. In the vicinity of the dynamical bifurcation point $i_{RF} = I_B$, the reflected signal phase ϕ depends critically on the input signal.

Figure 2. Poincare section of an RF-driven Josephson junction in the bistable regime ($\alpha = (1 - \omega/\omega_p) = 0.122$, $i_{RF}/I_B = 0.87$). The two stable oscillation states, labelled by 0 and 1, are indicated by white line segments. Point S which lies on the separatrix is the saddle point at which the escape trajectory from state 0 (dashed line) meets the retrapping trajectory into state 1 (solid line).

which describes the generalized force felt by the system is also plotted in the $(\delta_{\parallel}, \delta_{\perp})$ plane. Its value goes to zero at the attractors corresponding to states 0 and 1 and also at a third extremum which is the dynamical saddle point. Also shown in Fig. 2 is the calculated escape trajectory [12] from state 0 (dashed) and the corresponding retrapping trajectory [13] into state 1 (solid line). Fig. 2 has been computed for $\alpha = 0.122$, $Q = 20$ and $i_{RF}/I_B = 0.87$. These values correspond to typical operating conditions in our experiment. The dynamical switching from state 0 to 1 is characterized by a phase shift given here by $\tan^{-1} \left[(\delta_{\parallel}^1 - \delta_{\parallel}^0) / (\delta_{\perp}^1 - \delta_{\perp}^0) \right] = -139$ deg. Using the junction phase-voltage relationship and the transmission line equations, we can calculate the steady-state magnitude and phase of the reflected microwave drive signal. The change in the oscillation of δ results in a shift of the reflected signal phase $\Delta\phi_{01} = 89$ deg. Since there is no source of dissipation in the junction chip, there should be no change in the magnitude of the reflected signal power, even though $\sqrt{(\delta_{\parallel}^1 - \delta_{\parallel}^0)^2 + (\delta_{\perp}^1 - \delta_{\perp}^0)^2} \neq 0$.

Both static and dynamical switching can be described by an Arrhenius law in which the escape rate $\Gamma_{01} = (\omega_{att}/2\pi) \exp(-\Delta U/k_b T)$ is written as the product of an attempt frequency $\omega_{att}/2\pi$ and a Boltzman factor which contains the potential barrier height ΔU and the system temperature T . For the case of a DC current bias, the cosine potential, near the switching point, is approximated as a cubic potential with height $\Delta U_{st} = (4\sqrt{2}/3) \varphi_0 I_0 (1 - i_{DC}/I_0)^{3/2}$ where i_{DC} is the bias current. The attempt frequency is the plasma frequency ω_P . In the absence of fluctuations, the characteristic current at which switching occurs is I_0 . For the AC driven junction, the dynamical switching from oscillation state 0 to 1 can be cast in a similar form using the model of a particle in a cubic metapotential [4]. In this case, the effective barrier height is, to lowest order in $1/(\alpha Q)$, $\Delta U_{dyn} = u_{dyn} (1 - (i_{RF}/I_B)^2)^{3/2}$ with $u_{dyn} = 64\hbar/(18e\sqrt{3}) I_0 \alpha (1 - \alpha)^3$. The attempt frequency in the metapotential is given by $\omega_a = \omega_{a0} (1 - (i_{RF}/I_B)^2)^{1/2}$ with $\omega_{a0} = 4/(3\sqrt{3} RC) (\omega_p - \omega)^2$. The bifurcation current I_B where the 0 state ceases to exist is given by $I_B = 16/(3\sqrt{3}) \alpha^{3/2} (1 - \alpha)^{3/2} I_0$.

3. Devices and Setup

Typical junction fabrication parameters limit the plasma frequency to the 20 - 100 GHz range where techniques for addressing junction dynamics are inconvenient. We have chosen to shunt the junction by a capacitive admittance to lower the plasma frequency by more than an order of magnitude and attain a frequency in 1-2 GHz range (microwave L-band). In this frequency range, a simple on-chip electrodynamic environment with minimum parasitic elements can be implemented, and the hardware for precise signal generation and pro-

cessing is readily available. In the first step of sample fabrication, a metallic underlayer – either a normal metal (Au, Cu) or a superconductor (Nb) – was deposited on a silicon substrate to form one plate of the shunting capacitor, followed by the deposition of an insulating Si_3N_4 layer. Using e-beam lithography and double-angle shadow mask evaporation, we subsequently fabricated the top capacitor plates along with a micron sized $\text{Al}/\text{Al}_2\text{O}_3/\text{Al}$ tunnel junction. The critical current of the junction was in the range $I_0 = 1 - 2 \mu\text{A}$. By varying both the dielectric layer thickness and the pad area, the capacitance C was varied between 16 and 40 pF.

The junction + capacitor chip is placed on a microwave circuit-board and is wire-bonded to the end of a coplanar stripline which is soldered to a coaxial launcher affixed to the side wall of the copper sample box. We anchor the RF leak-tight sample box to the cold stage of a ^3He refrigerator with base temperature $T = 280 \text{ mK}$. The measurement setup is schematically shown in Fig. 3. Microwave excitation signals are coupled to the sample via the -13 dB side port of a directional coupler. The reflected microwave signal passes through the direct port of the coupler, and is amplified first using a cryogenic 1.20–1.85 GHz HEMT amplifier with noise temperature $T_N = 4 \text{ K}$. A DC bias current can be applied to the junction by way of a bias tee. We use cryogenic attenuators, isolators, and specially developed dissipative microstrip filters on the microwave lines in addition to copper-powder and other passive filters [6] on the DC lines to shield the junction from spurious electromagnetic noise. In the first set of experiments which probe the plasma resonance, a vector network analyzer was used to both source a CW microwave signal and to analyze the reflected power [14]. The dynamics of the transition between the two oscillation states was then probed using microwave pulses [15], generated by the amplitude modulation of a CW source with a phase-locked arbitrary waveform generator with 1 ns resolution. For the pulsed experiments, the reflected signal was mixed down to 100 MHz and digitally demodulated using a 2 GS/s digitizer to extract the signal phase ϕ .

4. Results

We first probed the drive current dependence of the reflected signal phase $\phi(i_{RF})$ by applying a $4 \mu\text{s}$ long symmetric triangular shaped pulse with a peak value $0.185 I_0$. The demodulated reflected signal was divided into 20 ns sections, each yielding one measurement of ϕ for a corresponding value of i_{RF} . The measurement was repeated 6×10^5 times to obtain a distribution of $\phi(i_{RF})$. In Fig. 4, the mode of the distribution is plotted as a function of i_{RF}/I_0 . For $i_{RF}/I_0 < 0.125$, the bifurcation amplifier is always in state 0, ϕ is constant and assigned a value of 0 deg. As the drive current is increased above $i_{RF}/I_0 = 0.125$, thermal fluctuations are sufficiently large to cause transitions

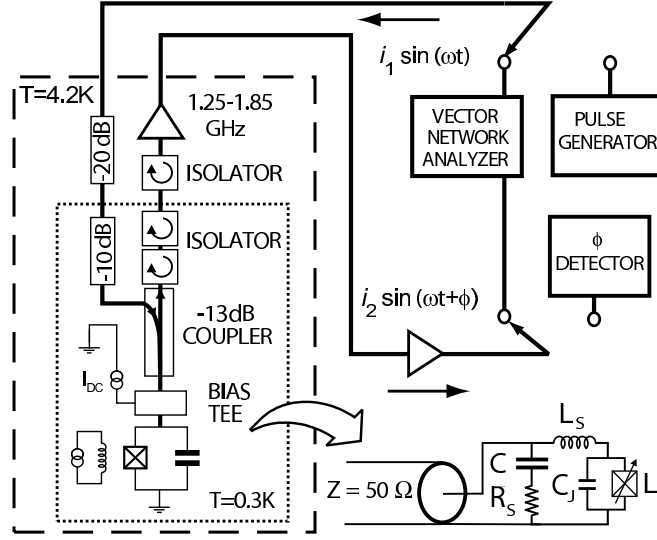


Figure 3. Schematic of the measurement setup. Thick lines correspond to $50\ \Omega$ coaxial transmission lines. The network analyzer is used for CW measurements. For probing the dynamics, the sample is switched to the pulse generator and phase detector. A lumped element model for the junction chip and measurement line is shown in the lower right. The two ideal current sources actually represent external sources.

to the 1 state. In the region between the two dashed lines at $i_{RF}/I_0 = 0.125$ and $i_{RF}/I_0 = 0.160$, ϕ displays a bimodal distribution with peaks centered at 0 and 74 deg with the latter corresponding to the amplifier in the 1 state. The dotted line in Fig. 4 is the average reflected signal phase $\langle\phi\rangle$. When i_{RF}/I_0 is increased above 0.160, the system is only found in state 1. In the decreasing part of the i_{RF} ramp, the system does not start to switch back to state 0 until $i_{RF}/I_0 = 0.065$. The critical switching currents I_B for the $0 \rightarrow 1$ transition and $I_{\bar{B}}$ for the $1 \rightarrow 0$ transition, calculated from numerical simulations to treat the inductance of wire bonds, are denoted with ticks in Fig. 4, and are in good agreement with experiment. The hysteresis $I_{\bar{B}} < I_B$ is a consequence of the asymmetry in the escape barrier height for the two states. Thus, the $0 \rightarrow 1$ transition at $i_{RF} = I_B$ is nearly irreversible, allowing the bifurcation amplifier to latch and store its output during the integration time set by the sensitivity of the follower amplifier.

To determine the sensitivity of the bifurcation amplifier, we have characterized in detail the switching in the vicinity of the $0 \rightarrow 1$ transition. We excited the system with two different readout pulse protocols. In the first protocol, the drive current was ramped from 0 to its maximum value in 40 ns and was then held constant for 40 ns before returning to 0. Only the final 20 ns of the constant drive period were used to determine the oscillation phase with the first

20 ns allotted for settling of the phase. Histograms taken with a 10 MHz acquisition rate are shown in Fig. 5. In the upper panel, the two peaks corresponding to states 0 and 1 can easily be resolved with a small relative overlap of 10^{-2} . The width of each peak is consistent with the noise temperature of our HEMT amplifier. In this first method, the latching property of the system has not been exploited. In our second protocol for the readout pulse, we again ramp for 40 ns and allow a settling time of 20 ns, but we then reduce the drive current by 20% and measure the reflected signal for 300 ns. In that latter period, whatever state was reached at the end of the initial 60 ns period is "latched" and time is spent just increasing the signal/noise ratio of the reflected phase measurement. As shown in the lower panel of Fig. 5, the two peaks are now fully separated, with a relative overlap of 6×10^{-5} allowing a determination of the state 1 probability with an accuracy better than 10^{-3} . This second protocol would be preferred only for very precise time-resolved measurements of I_0 or for applications where a low-noise follower amplifier is impractical.

A third experiment was performed to study the state 1 switching probability $P_{01}(i_{RF})$ for different values of the temperature T and I_0 , the latter being varied with a magnetic field applied parallel to the junction plane. Using the

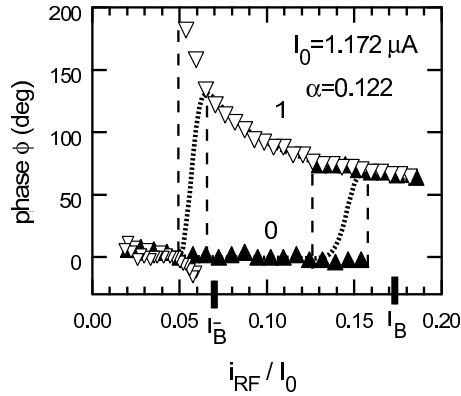


Figure 4. Hysteretic variation of the reflected signal phase ϕ with drive current i_{RF}/I_0 . Symbols denote the mode of ϕ , with up and down triangles corresponding to increasing and decreasing $i_{RF} = I_B$, respectively. The dotted line is $\langle \phi \rangle$. The calculated bifurcation points, $I_{\bar{B}}$ and I_B , are marked on the horizontal axis. The 0 and 1 phase states are reminiscent of the superconducting and dissipative states of the DC current biased junction.

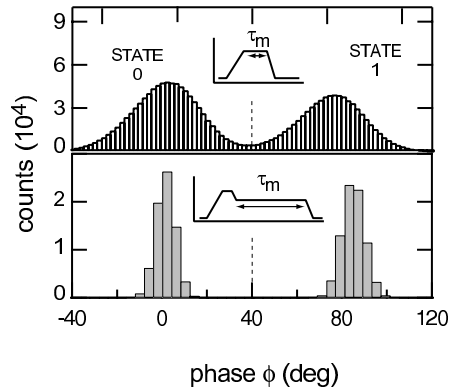


Figure 5. Histograms of the reflected signal phase ϕ at $i_{RF}/I_0 = 0.145$. The upper histogram contains 1.6×10^6 counts with a measurement time $\tau_m = 20$ ns. The lower panel, taken with the latching technique, has 1.5×10^5 counts with a measurement time $\tau_m = 300$ ns. Data here has been taken under the same operating conditions as in Fig 4. The dashed line represents the discrimination threshold between the 0 and 1 state.

first readout protocol and the discrimination threshold shown in Fig. 5, we obtain the switching probability curves shown in Fig. 6. Defining the discrimination power d as the maximum difference between two switching probability curves which differ in I_0 we find that at $T = 280$ mK, $d = 57\%$ for $\Delta I_0/I_0 = 1\%$ – the typical variation observed in a superconducting charge-phase qubit [16]. The switching probability curves should shift according to $(\Delta I_B/I_B)/(\Delta I_0/I_0) = 3/(4\alpha) - 1/2 + O(1/(\alpha Q)^2)$, which for our case takes the value 5.6. In Fig. 6, the curves are shifted by 6%, which agrees well with this prediction. For the case of the DC current biased junction, similar curves would shift only by 1% since the switching current is I_0 itself. Comparable discrimination power using DC switching has only been achieved in these devices at $T \leq 60$ mK. As the temperature is increased, the switching probability curves broaden due to increased thermal fluctuations and the discriminating power decreases: at $T = 480$ mK, $d = 49\%$.

Finally, we determined the escape rate $\Gamma_{01}(i_{RF}, I_0, T)$ as a function of i_{RF} by measuring the time dependence of the switching probability, using a method previously applied to the determination of the static switching rates to the voltage state [17]. After the initial ramp (40 ns) and settling period (20 ns), the reflected signal phase was extracted every 20 ns for a duration of 1 μ s. By repeating this measurement, we generated switching probability histograms which we analyzed as $P_{01}(t) = 1 - \exp(-\Gamma_{01} \cdot t)$. To obtain the escape rate at different temperatures, two different techniques were used. In the first method, we varied the temperature of the cryostat and used a magnetic field to keep the critical current constant at $I_0 = 1.12 \mu$ A. In the second method, I_0 was kept fixed at 1.17 μ A, and a 1 – 2 GHz white noise source irradiating the junction was used to increase the effective temperature. In Fig. 7 we show the drive current dependence of the escape rate as $(\ln(2\pi\omega_a/\Gamma_{01}))^{2/3}$ plotted versus i_{RF}^2 for two different sample temperatures. Data in this format should fall on a straight line with a slope $s(T)$ proportional to $(u_{dyn}/k_B T)^{2/3}$. A trace taken at $T = 500$ mK is also shown in Fig 7.

In parallel with these dynamical switching measurements, we ran static switching measurements to obtain an escape temperature T_{st}^{esc} . Due to insufficient filtering in our RF amplifier line outside the measurement band, T_{st}^{esc} exceeded T by 60 mK. Using u_{dyn}^{calc} and $s(T)$ we can cast the results of the dynamical switching measurements into a dynamical escape temperature $T_{dyn}^{esc} = u_{dyn}^{calc}/k_B s(T)^{3/2}$. We plot T_{dyn}^{esc} versus T_{st}^{esc} in the inset of Fig. 7. The agreement is very good, and only deviations at the highest temperatures are observed. Analyzing the dynamical switching data with T_{st}^{esc} in place of T , we extract a value of $u_{dyn} = 10.7$ K from the $T = 280$ mK data with $I_0 = 1.17 \mu$ A while the calculated value keeping higher order terms in $1/\alpha Q$ is $u_{dyn}^{calc} = 11.0$ K.

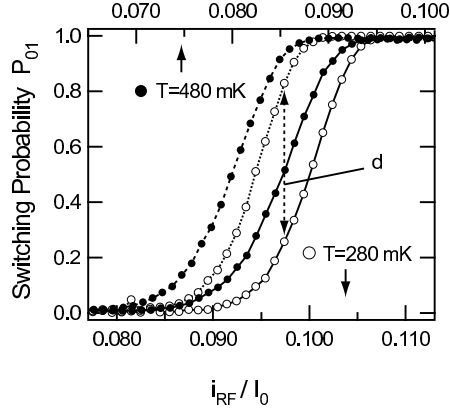


Figure 6. Switching probability curves at $T = 280$ mK and $T = 480$ mK as a function of the drive current i_{RF} . The discrimination power d is the maximum difference between two curves at the same temperature which differ by approximately 1% in I_0 .

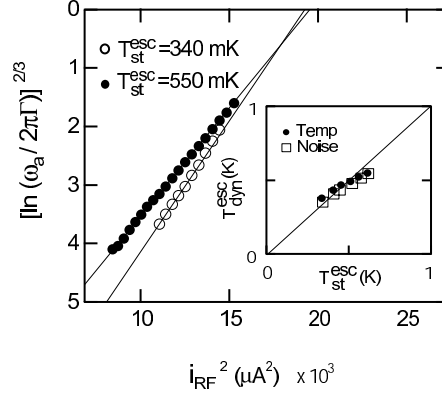


Figure 7. Escape rate as a function of drive power for two different operating temperatures with $I_0 = 1.12 \mu\text{A}$. The inset shows the relationship between dynamic and static escape temperatures when varying either the sample temperature or the injected noise power.

5. Conclusion

With the JBA operating at $T_{st}^{esc} = 340$ mK, it is possible to resolve with a signal/noise ratio of 1 a 10 nA variation in I_0 in a total time ≤ 80 ns, corresponding to a critical current sensitivity of $S_{I_0}^{1/2} = 3.3 \times 10^{-6} \text{ A} \cdot \text{Hz}^{-1/2}$. This value is in agreement with the prediction from the analytical theory $S_{I_0}^{1/2} = \eta(i_{RF}/I_0, \alpha) (k_B T / \varphi_0) \cdot \tau_m^{1/2}$, where $\eta \approx 1.4$ near the bifurcation point and $\varphi_0 = \hbar/2e$. The advantage of the bifurcation amplifier over SQUIDs [18] resides in its extremely low back-action. Since there is no on-chip dissipation, the only source of back-action is the matched isolator load, which is efficiently thermalized at $T = 280$ mK. An important point is that in the JBA, only fluctuations from the load that occur in a narrow band centered about the plasma frequency contribute to the back-action, whereas in the SQUID noise from many high frequency bands is also significant. Finally, the bifurcation amplifier does not suffer from quasiparticle generation associated with hysteretic SQUIDs [2] and DC current-biased junctions [3] which switch into the voltage state. Long quasiparticle recombination times at low temperatures limit the acquisition rate of these devices while the recombination process itself produces excess noise for adjacent circuitry [19].

In conclusion, the JBA is competitive with the SQUID for applications where low back-action is required. Its speed, suppression of on-chip dissi-

pation, and latching make it ideal for the readout of superconducting qubits. At temperatures such that $T_{dyn}^{esc} \leq 60$ mK, the discrimination power would be greater than 95%, hence permitting stringent tests of Quantum Mechanics, like the violation of Bell's inequalities.

Acknowledgments

We would like to thank D. Prober, E. Boaknin, M. Dykman, L. Grober, D. Esteve, D. Vion, S. Girvin and R. Schoelkopf for discussions and assistance. This work was supported by the ARDA (ARO Grant DAAD19-02-1-0044), the NSF (Grant ITR DMR-0325580, DMR-0072022), and the Keck foundation.

References

- [1] B. Josephson, Rev. Mod. Phys. 36, 216 (1964).
- [2] I. Chiorescu, Y. Nakamura, C.J.P.M. Harmans, and J.E. Mooij, Science 299, 5614 (2003).
- [3] A. Cottet, D. Vion, A. Aassime, P. Joyez, D. Esteve, and M.H. Devoret, Physica C 367, 197 (2002).
- [4] M.I. Dykman and M.A. Krivoglaz, Physica A 104, 480 (1980).
- [5] M.H. Devoret, D. Esteve, J.M. Martinis, A. Cleland, and J. Clarke, Phys. Rev. B 36, 58 (1987).
- [6] J.M. Martinis, M.H. Devoret, and J. Clarke, Phys. Rev. B 35, 4682 (1987).
- [7] B. Yurke, L.R. Corruccini, P.G. Kaminsky, L.W. Rupp, A.D. Smith, A.H. Silver, R.W. Simon, and E.A. Whittaker, Phys. Rev. A 39, 2519 (1989).
- [8] T. Holst and J. Bindslev Hansen, Physica B 165-166, 1649 (1990).
- [9] L.D. Landau and E.M. Lifshitz, Mechanics (Reed, Oxford, 1981).
- [10] T.A. Fulton and L.N. Dunkleberger, Phys. Rev. B 9, 4760 (1974).
- [11] R.L. Kautz, Phys. Rev. A 38, 2066 (1988).
- [12] M.I. Dykman and M.A. Krivoglaz, JETP 50, 30 (1980).
- [13] A.P. Dmitriev, M.I. D'yakonov, and A.F. Ioffe, JETP 63, 838 (1986).
- [14] I. Siddiqi, R. Vijay, F. Pierre, C.M. Wilson, L. Frunzio, M. Metcalfe, C. Rigetti, R.J. Schoelkopf, M.H. Devoret, D. Vion, and D.E. Esteve, arXiv:cond-mat/0312553 v1 21 Dec 2003.
- [15] I. Siddiqi, R. Vijay, F. Pierre, C.M. Wilson, M. Metcalfe, C. Rigetti, L. Frunzio, and M.H. Devoret, arXiv:cond-mat/0312623 v1 23 Dec 2003.
- [16] D. Vion, A. Aassime, A. Cottet, P. Joyez, H. Pothier, C. Urbina, D. Esteve, and M. Devoret, Science 296, 886 (2002).
- [17] C. Urbina, D. Esteve, J.M. Martinis, E. Turlot, M.H. Devoret, H. Grabert, and S. Linkwitz, Physica B 169, 26 (1991).
- [18] M. Muck, J.B. Kycia, and J. Clarke, Appl. Phys. Lett. 78, 967 (2001).
- [19] J. Mannik and J.E. Lukens, arXiv:cond-mat/0305190 v2 6 Nov 2003.